PHYSICAL REVIEW A VOLUME 19, NUMBER 4 APRIL 1979

Determination of Fe charge-state distributions in the Princeton large torus by Bragg crystal x-ray spectroscopy

K. W. Hill, S. von Goeler, M. Bitter, L. Campbell, R. D. Cowan,* B. Fraenkel,† A. Greenberger, R. Horton, J. Hovey, W. Roney, N. R. Sauthoff, and W. Stodiek

Plasma Physics Laboratory, Princeton University, Princeton, New Jersey 08540

(Received 10 July 1978)

A curved-crystal Bragg x-ray spectrometer has been used to measure $K\alpha$ or $1s$-$2p$ radiation from highly stripped Fe XVIII-Fe XXV impurity ions in the Princeton large torus tokamak. The spectrometer has sufficient energy resolution ($\lesssim 4$ eV at 6400 eV) to distinguish between the different ionization states of iron by measuring the energy shift of the $K\alpha$ x rays. The measured wavelengths agree well with theory and with spectra from solar flares and from laser-produced plasmas. The distribution of Fe charge states in the center of the discharge has been inferred from a comparison of the measured x-ray spectrum with theory. The shape of the spectrum depends strongly on electron temperature (T_e) in the range T_e = 800–1500 eV. Within the factor of 2 uncertainty in L-shell ionization cross sections, measured intensities agree with theory, which is based on coronal equilibrium, indicating that the ion lifetime in the center of the plasma is approximately equal to or greater than the equilibration time.

I. INTRODUCTION

Impurities in tokamaks are located in shells of different charge states around the center of the discharge. The distribution of charge states depends mainly on the electron temperature T_e of the discharge. Since the cross section for production of impurity x-ray line radiation can vary significantly with charge state, it is necessary to know this charge-state distribution in order to accurately determine the concentration and radial variation of an impurity by measurement of its line radiation.

A convenient means for measuring this charge-state distribution for iron ions is to measure the energy shift of the Fe $K\alpha$ or $1s$-$2p$ x-ray line relative to the energy of x rays emitted by the unstripped Fe.[1] For each L-shell electron removed between charge states Fe^{17+} to Fe^{24+}, the average $1s$-$2p$ x-ray energy increases by ~40 eV.[2,3] In the present experiment on the Princeton large torus (PLT), the Fe $K\alpha$ energy shifts have been measured by means of a Bragg curved-crystal x-ray spectrometer having an energy resolution of $\lesssim$4-eV full width at half maximum (FWHM), thus permitting not only distinction between charge states, but also observation of multiplet structure in the $1s$-$2p$ x rays. The spectrometer uses a position-sensitive detector on the Rowland circle to permit simultaneous measurement of x rays from a 500-eV wide band of energies. The results are compared with detailed calculations of Merts *et al.*,[2,3] which predict (i) the distribution of charge states in coronal equilibrium and (ii) the cross sections for excitation of the $1s$-$2p$ transition via both direct collisional excitation and dielectronic recombination. A major aim of the measurements is to experimentally test the validity and accuracy of theoretical predictions based on coronal equilibrium and their applicability to tokamak plasmas.

The experimental arrangement and data accumulation procedure are discussed in Sec. II. In Sec. III, spectra from PLT are compared with theoretical spectra[2-4] and with other experiments[4-6] to demonstrate the correspondence between observed and calculated line positions. In Sec. IV, charge-state distributions are inferred from the measured spectra by comparison with theoretical calculations.[2,3]

II. EXPERIMENTAL ARRANGEMENT

The instrument used for these measurements was a curved-crystal Bragg spectrometer as shown schematically in Fig. 1. X rays from the center of the plasma pass through a beryllium window into a helium-filled phenolic tube. They are diffracted and focused by the crystal onto a multiwire proportional counter.

The x-ray window is a 3.5 cm × 9 cm × 0.0015 in. Be foil which is supported against the external atmospheric pressure by a slotted stainless-steel structure. This window transmits ≈99% of the x rays, whereas an air path of the same length would transmit only ~0.2% of the radiation.

The principle of operation of the crystal diffracting element is illustrated schematically in Fig. 1. In order to be diffracted by the crystal, an x ray of wavelength λ must strike the surface at an angle of θ_0 (relative to the surface) which satisfies the Bragg relation $n\lambda = 2d\sin\theta_0$, where n is the diffraction order ($n = 1$ in the present experiment) and d

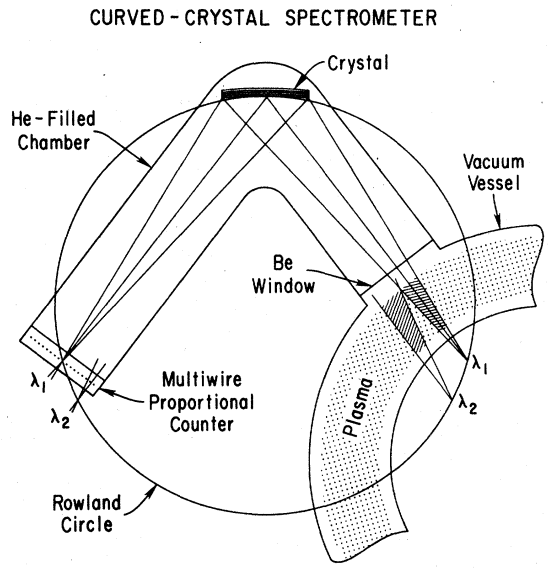

FIG. 1. Schematic drawing of curved-crystal spectrometer. X rays from the plasma pass through the Be window into the He-filled tubes where they are diffracted by the crystal and focused onto the detector, a position-sensitive, multiwire proportional counter. The crystal will diffract only those x rays from the upper shaded region of the plasma having wavelength λ_1 satisfying the Bragg relation $\lambda_1 = 2d\sin\theta_1$, where d is the spacing between crystal lattice planes and θ_1 is the angle between the x rays and a tangent to the crystal surface. In order to satisfy the Bragg relation also, other wavelengths such as λ_2 must originate from other regions of the plasma, such as the lower shaded region. Thus x rays of different λ fall at different positions along the position-sensitive detector.

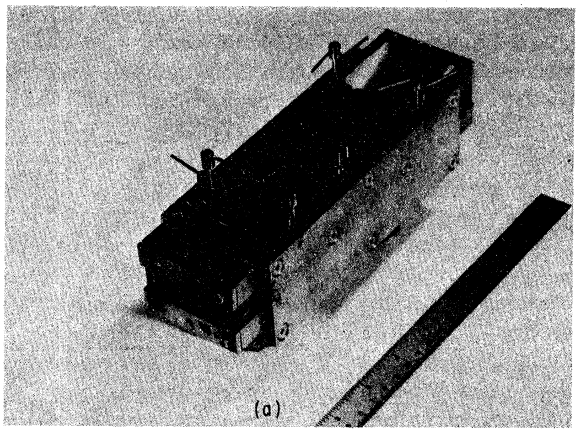

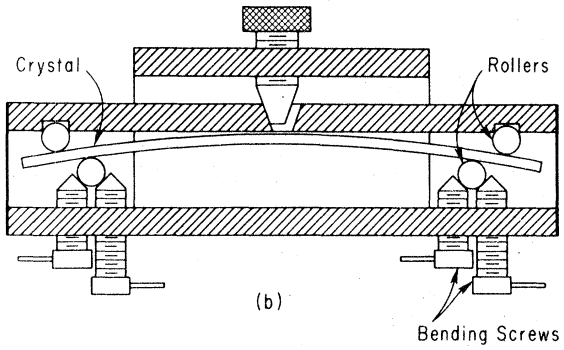

FIG. 2. (a) Photograph of the Ge(220) crystal in its bending jig. The crystal, two rollers, and eight screws for adjusting the radius of curvature can be seen. (b) Schematic cross-sectional illustration of crystal-bending jig showing a side view of the bent crystal slab. The two front (lower) cylindrical rollers press against the front (concave) surface of the crystal while the rear surface is held fixed by the two rear rollers. The radius of curvature of the crystal is adjusted by means of the fine-thread screws which hold the front rollers. The rear screw permits a lateral displacement of the rear rollers relative to the front ones so that the crystal can be bent to either a cylindrical or a logarithmic-spiral contour.

is the spacing between crystal lattice planes. In Fig. 1 only x rays of wavelength λ_1 emitted from ions in the upper shaded region of the plasma will be diffracted by the crystal and focused to the point of the detector labeled λ_1. Another wavelength λ_2 will be accepted from ions in the lower shaded region and focused to point λ_2 of the detector. The use of a position-sensitive detector, then, permits one to measure simultaneously a range of x-ray wavelengths or energies spanning, in the present case, the region from 6.3 to 6.85 keV.

The Johann-geometry[7] crystal provides nearly exact focusing of uncollimated, nonmonochromatic x rays. A 6×1.5 in.^{2} germanium (220) crystal is bent by a four-bar bending jig (Fig. 2) to a radius of curvature $2R$. X rays of wavelength $\lambda = (2d/n)\sin\theta_0$ are reflected at the Bragg angle θ_0 and focused onto the Rowland circle of radius R. Position along the Rowland circle x is a sensitive function of λ: for our apparatus, with $n=1$, $2d = 4.000$ Å, $R = 2.42$ m, $\lambda \approx 1.85$ Å, and $\theta_0 = 28°$, the dispersion is

$$\frac{dx}{d\lambda} = \frac{nR}{d\cos\theta_0} \approx 137 \text{ cm/Å}. \quad (1)$$

Figure 2(a) shows a picture of the crystal located in the bending jig. The two front rollers and the eight screws which are used to adjust the position of the rollers can be seen. A schematic cross-sectional view of the jig is shown in Fig. 2(b). The cone-shaped screw at the back of the jig offsets the two rear rollers laterally relative to the front rollers in order to bend the crystal into a logarithmic spiral instead of a cylinder. This feature provides the possibility of avoiding the Johann geo-

metrical focusing defect, but was not used in the present experiment. The exact focusing Johansson geometry[8] was not used due to difficulties in grinding the surfaces to the tolerances required. These details are discussed more fully in Refs. 7–9.

The x rays are detected by a position-sensitive multiwire proportional counter[10] with a 2×4 in.^{2} thin Myler entrance window. The counter has anode wires along the 4-in. window dimension and has approximately 100 cathode wires with 1-mm separation running perpendicular to the anode wires, as illustrated in Fig. 3. One end of each cathode wire is capacitively coupled to a wound delay line. An x-ray photon ionizes the $P10$ gas mixture, producing an electron avalanche to an anode wire. Image pulses are induced on cathode wires and transmitted to the delay line, where they propagate towards both ends of the line with a velocity depending upon the construction of the line. Standard electronics convert the difference in arrival time of the pulses at the ends of the delay line into a pulse whose amplitude depends linearly on the position at which the photon struck the detector. These pulses go into a pulse-height analyzer which provides a 255-channel display of photon count versus pulse height (position).

The pulse-height analyzer is controlled by the PDP-10 computer, which also reads and stores the spectra on disk files for later analysis. Four complete spectra can be taken during a single ~0.6-sec PLT discharge.

The position resolution and linearity of the detector were checked by placing an array of apertures before the detector window and illuminating it with an ^{55}Fe source. The best position resolution obtained was $\lesssim 0.4$ mm, and the detector was linear within this position uncertainty.

The energy resolution of the spectrometer was measured with an iron x-ray tube, using the $K\alpha_1$ line at 6404 eV. This experiment indicated an energy resolution of ~3.5-eV FWHM. The natural linewidth is 2.35 eV. The contribution to the measured linewidth from the minimum position resolution of the detector is 2.0-eV FWHM and that from the rocking curve width (16 arcsec at $\lambda = 1.9$ Å)[11] of the Ge(220) crystal is 0.9 eV. Other possible sources of line broadening are (a) the Johann geometrical aberration,[7] (b) deviation of the detector from the Rowland circle, (c) the nonzero depth of the detector, (d) nonuniform curvature of the crystal, and (e) perpendicular divergence.[12] The line broadening due to effects (a), (b), and (c)

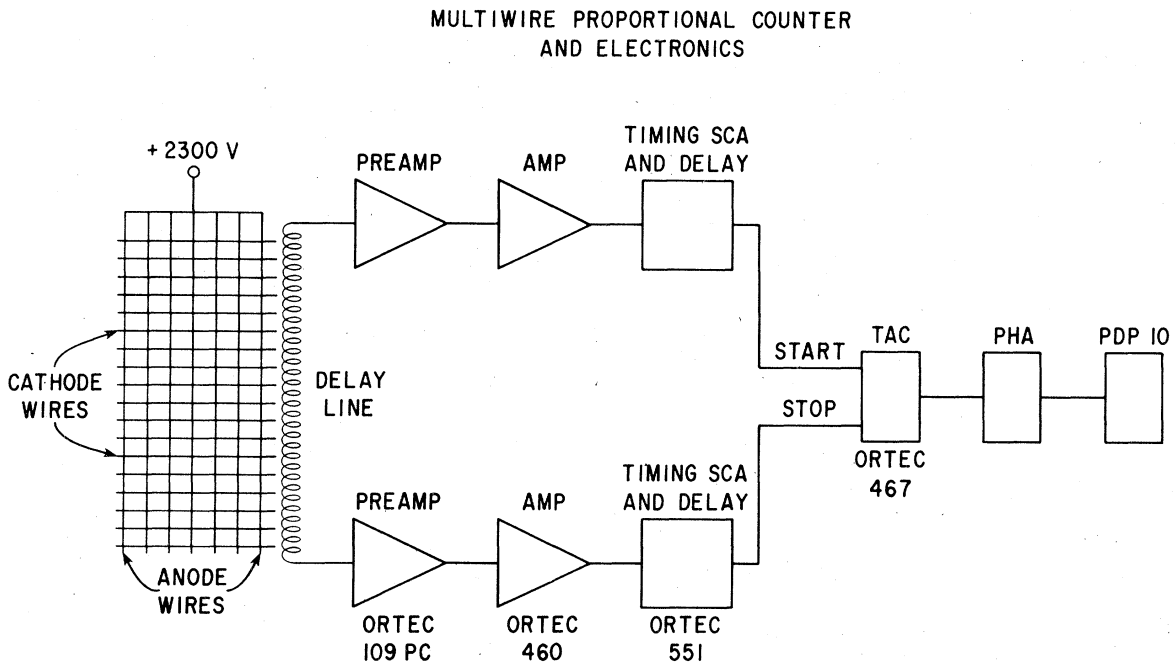

FIG. 3. Schematic diagram of the multiwire proportional counter and electronics. An x ray produces an electron avalanche on an anode wire. This induces image signals on the nearest cathode wires, which are capacitively coupled to the delay line, with the difference in time of arrival at the two ends being proportional to the position at which the x ray struck the detector. The time-to-amplitude converter (TAC) converts this time difference to a pulse whose amplitude depends linearly on the position at which the x ray struck the detector. These pulses are digitized and stored by the pulse-height analyzer (PHA) and later read by the PDP-10 computer.

can be decreased by reducing the effective length of the crystal. For the full usable crystal length of ~9 cm in the present experiment they contribute, respectively, 0.9, 2.4, and 0.3 eV to the x-ray linewidth. However, for most plasma discharges, especially for those with the electron temperature $T_e(0) > 1200$ eV, a two-blade aperture limited the effective length of the crystal to only ~0.5–2.0 cm. For a 1-cm effective length, broadening due to effects (a), (b), and (c) is reduced to 0.01, 0.03, and 0.04 eV, respectively. The broadening due to effect (d), nonuniform curvature of the crystal, was measured by illuminating different parts of the crystal and checking the position of the x-ray line. A large shift of the line was observed for diffraction from near one end of the crystal; for most of the spectra this section of the crystal was blocked off and only the remaining portion, which had uniform curvature (line shift <1 eV) was used. Perpendicular divergence[12] (e) is small in the present experiment because the ratio of Rowland circle radius to crystal height is large.

III. COMPARISON OF MEASURED LINE POSITIONS WITH CALCULATIONS AND OTHER EXPERIMENTS

An overview of the x-ray emission from PLT in the energy range 1–15 keV is provided by the lower-resolution pulse-height-analysis system (PHA), using cooled Si (Li) detectors. A typical spectrum is shown in Fig. 4(a). This system provides, from the slope of the bremsstrahlung and recombination continuum, a time-dependent measure of the electron temperature T_e, as shown in Fig. 4(b), and can be scanned radially from shot to shot. More importantly, for the present studies, the PHA system is absolutely calibrated so that the x-ray line radiation intensity from impurity ions can be accurately determined. Of particular interest for the present experiment is the Fe $K\alpha$ peak in Fig. 4(a) which is the object of our study. Since the PHA has an energy resolution of only ~200-eV FWHM, the $K\alpha$ x-ray lines from the different charge states are blended together into one broad peak.

The curved-crystal spectrometer emphasizes the region of Fig. 4(a) from 6300 to 6850 eV with an energy resolution of ~4-eV FWHM. Four spectra taken with this instrument during a single shot of 500-msec duration are shown in Fig. 5. Each spectrum is a graph of number of x-ray photons versus x-ray energy. The four spectra were integrated during successive 125-msec intervals of the shot as indicated above the graphs. Also indicated are the total number of x-ray photons recorded during each interval (TC) and the average count rate (RATE) in photons per millisecond. An expanded example

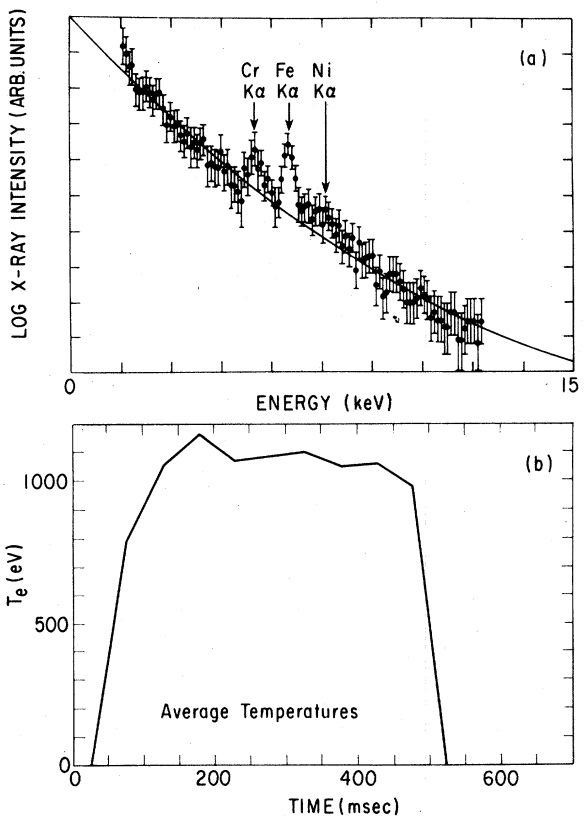

FIG. 4. (a). Typical x-ray spectrum taken with the PLT cooled Si (Li) pulse-height-analysis (PHA) system. $K\alpha$ peaks from the major components of the stainless-steel vacuum vessel can be seen. Up to 14 such spectra can be recorded during a single discharge. (b) Time history of electron temperature during a discharge. The temperatures were obtained from the slopes of the continua of 10 spectra such as those shown in (a) above. Each spectrum covered a 50-msec portion of a 500-msec shot.

of one of these typical spectra is the dashed curve in Fig. 6, which also shows the correspondence between observed and calculated line positions. The theoretical[2,3] spectrum (solid curve) was shifted toward lower energy by only 11 eV (< 0.2%), indicating the remarkable accuracy of the calculations. The major peaks correspond mainly to given charge states which are indicated by Roman numerals (spectroscopic notation). Strictly speaking, it is not possible to associate a spectral peak with a given charge state. First, multiplet splitting results in a structure within each major peak; in some regions these multiplet components overlap components of a neighboring peak. More importantly, however, a given charge state (Fe XXII, for instance) can produce radiation under three major peaks (e.g., those labeled XXI, XXII, and XXIII). The reason for this is that the major peak under

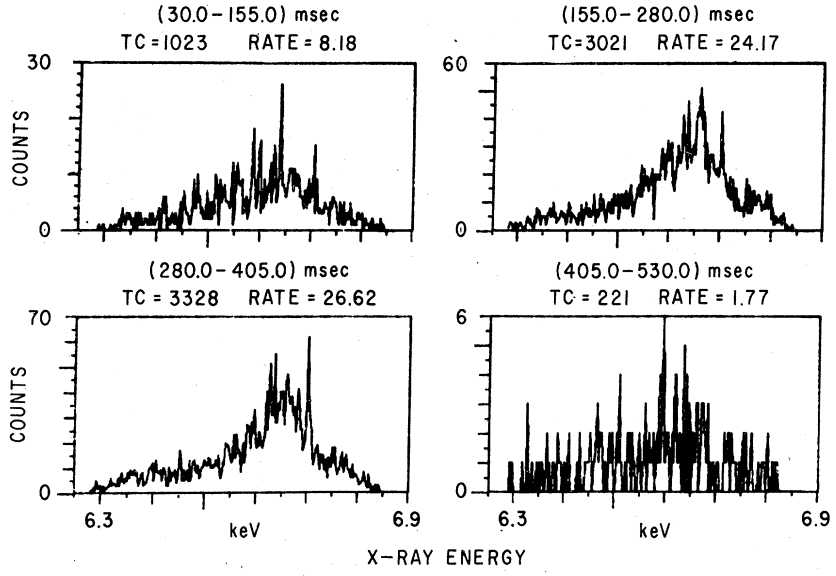

FIG. 5. Typical display of spectra taken with the curved-crystal spectrometer during one discharge of PLT. The abcissas indicate x-ray energy and the ordinates indicate the number of photons detected at each energy. As the labels above the spectra indicate, accumulation of the first spectrum was begun at $t=30$ msec after the beginning of the discharge and ended at $t=155$ msec; the remaining three spectra were recorded during the next three successive intervals of 125-msec duration. The label TC indicates the total number of photons registered and RATE is the average count rate in photons per millisecond. Note that during the first three time quadrants, the count rate is increasing, and the centroid of the x-ray peaks is shifting toward higher energy, indicating more highly stripped iron ions. During the fourth time quadrant, the discharge has cooled considerably, and fewer x rays are observed.

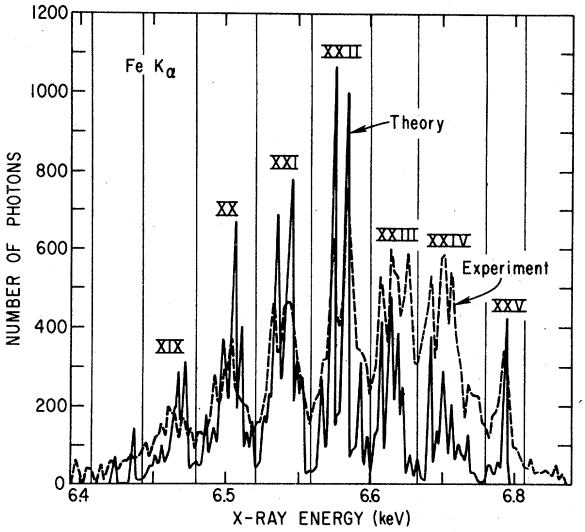

FIG. 6. Typical Fe $K\alpha$ spectrum from PLT (dashed curve) compared with a theoretical spectrum (solid curve) generated by Merts *et al.* (Ref. 2). The theoretical spectrum has been shifted toward lower energy by 11 eV (< 0.2%). The major peaks corresponding to a given charge state are indicated by Roman numerals. Differences between theory and experiment in the subpeak locations (due to multiplet splitting) of a given charge state are within the uncertainty expected for the calculations.

which a $K\alpha$ line falls depends mainly upon the number of L-shell electrons present when the $2p \rightarrow 1s$ transition occurs. An Fe XXII ion, for example, may be collisionally excited into either the $1s2s^22p^2$ state, resulting in radiation under the Fe XXII peak, or into a $1s2s^22pnl$ $(n>2)$ state, resulting in radiation near the Fe XXIII peak.

$$1s^22s^22p \rightarrow \begin{cases} 1s2s^22p^2 \rightarrow 1s^22s^2p \\ (\text{XXII peak}) \\ 1s2s^22pnl \rightarrow 1s^22s^2nl \\ (\text{XXIII peak if } n>2). \end{cases} \tag{2}$$

Similarly, excitation of an Fe XXII ion by dielectronic recombination into Fe XXI can result in radiation near the Fe XXI, Fe XXIII, or Fe XXIII peaks.

$$1s^22s^2p + e \rightarrow \begin{cases} 1s2s^22p^3 \rightarrow 1s^22s^22p^2 \\ (\text{XXI peak}) \\ 1s2s^22p^2nl \rightarrow 1s^22s^22pnl \\ (\text{XXII peak if } n>2) \\ 1s2s^22pnln'l' \rightarrow 1s^22s^2nln'l' \\ (\text{XXIII peak if } n,n'>2). \end{cases} \tag{3}$$

It will be understood that, e.g., the designation Fe XXII peak refers to the peak labeled XXII in Fig. 6 even though it cannot be strictly associated with radiation from only the Fe XXII ion. These complications result in a complex substructure which is reproduced in the theoretical curve of Fig. 6, and which is in surprisingly good agreement with the experiment. Differences between theory and experiment in the relative energies of multiplet peaks of a given charge state are within the 10% uncertainty expected for the calculation of the multiplet splitting.

Some differences between the theoretical and experimental spectra of Fig. 6 are evident. First, the theoretical spectrum appears slightly compressed along the energy scale, relative to experiment. The discrepancy is less than 5% and may be attributed to small systematic errors in calculation of the energy levels of the different charge states. Also, uncertainties of a few percent may exist in the relative energy calibration of the spectrometer. The calibration was accomplished by locating the Fe $K\alpha_1$ line at 6.404 keV from an x-ray tube and calculating the energy scale from the $2d$ spacing of the crystal (4.00 Å) and the distance between detector and crystal. Secondly, the theoretical spectrum has less intensity in the valleys between major peaks than does the experiment. This is mostly due to the fact that the theoretical spectrum was calculated with a narrower linewidth than the experimental one in order to emphasize the multiplet peak energy positions; however, this discrepancy persisted also when the calculation was performed with broader linewidth. Improper subtraction of background from the experimental spectrum could contribute to the higher observed intensities in the valleys. There may also be significant contributions from transition arrays omitted in the calculations. Only cases $nl = 3s$, $3p, 3d, 4p, 5p$ in (2) and (3) were included; the third case in Eq. (3) was omitted entirely. Another possible contribution to the measured background and to other discrepancies between measured and calculated intensities is the $K\beta$ spectrum from chromium ions, part of which falls in the Fe $K\alpha$ range.

Both the relative multiplet peak positions and the relative multiplet peak intensities for a given charge state are in remarkable agreement with theory. Discrepancies which do exist in intensity can result from uncertainties in the calculation of transition rates; also, collisional excitation predicts a different distribution of intensities among components of a given transition array than does dielectronic excitation. A different balance between the two types of excitation could significantly alter the relative multiplet intensities.

To further verify the accuracy of the measured peak locations, Fig. 7(a) compares a spectrum from PLT at a peak electron temperature of 1500 eV with a Fe $K\alpha$ spectrum measured from a solar flare[4,5] at an estimated temperature of 2000 eV. Although the flare spectrum has lower background and somewhat better energy resolution, the major features agree very well. The vertical solid and dashed lines represent positions and intensities of various transitions as identified and discussed in Ref. 4. The flare spectrum was shifted so that the He-like Fe XXV resonance line w coincides with the present experiment.

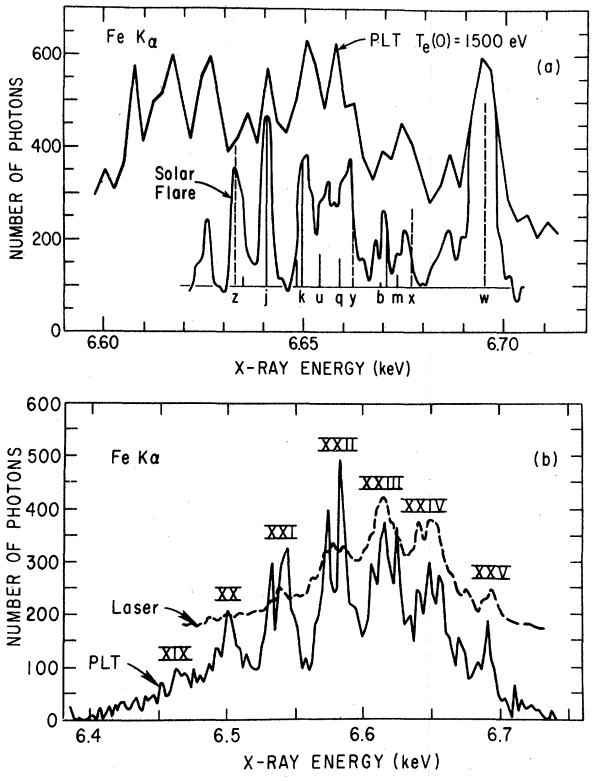

FIG. 7. (a). Comparison of a portion of an Fe $K\alpha$ spectrum from PLT (upper curve) at $T_e(0) = 1500$ eV with a spectrum recorded from a solar flare (lower curve) at estimated T_e of 2000 eV by Grineva *et al.* (Ref. 5). The solar-flare spectrum has been shifted downward in energy by 7 eV so that the He-like resonance line (labeled w) at a quoted wavelength value of 1.85 Å or 6701.7 eV coincides with the current measured value of 6695 eV. The vertical lines represent x-ray line positions taken from Ref. 4 for several components of He-like (dashed lines) and Li-like (solid lines) Fe $1s$-$2p$ transitions. The line identification scheme is also summarized in Ref. 4. (b) Comparison between a Fe $K\alpha$ spectrum from PLT at $T_e(0) = 1000$ eV, $n_e \approx 5 \times 10^{13}$ cm^{-3} and one from a laser-produced plasma (lower curve) at $T_e = 830$ eV, $n_e = 10^{21}$ cm^{-3} (Ref. 6). Higher charge states are indicated in the laser-produced plasma even though T_e is lower.

Figure 7(b) shows a comparison between Fe $K\alpha$ spectra from PLT measured at $T_e(0) = 1000$ eV, $n_e \approx 5\times 10^{13}$ cm^{-3} and from a laser-produced plasma[6] at $T_e = 830$ eV, $n_e = 10^{21}$ cm^{-3}. The Fe XXI – Fe XXV peak groups agree remarkably well in energy position. The distribution of peak intensities, however, is shifted toward higher charge states in the laser-produced plasma, which probably is related to the fact that the equilibrium is slightly different for the higher densities encountered in the laser plasma.

IV. MEASURED CHARGE-STATE DISTRIBUTIONS

In order to obtain charge-state concentrations from the experimental spectra, we require a model which accounts for the rates of excitation of the various $1s$-$2p$ transitions possible for a given charge state and also accurate calculations of the charge-state distribution of Fe ions at T_e values typical for tokamaks, under the assumption of coronal equilibrium (an assumption which is thought to be marginally satisfied in typical PLT discharges). For both processes there exists, of course, a long list of papers with important contributions. The coronal model[2] has been improved markedly since the time of Elwert,[13] mostly by incorporating dielectronic recombination (Burgess)[14] in the computations (Jordan).[15] As far as the $1s$-$2p$ transition is concerned, it was Gabriel's[16] discovery of the importance of dielectronic excitation for high-Z ions which made quantitative comparison between theory and experiment possible. At present, the most extensive calculations for both processes are those of Merts, Cowan, and Magee,[2] which we will use in our paper. The weakest link in the calculations of coronal equilibrium are the ionization cross sections. In general, the semiempirical cross sections of Lotz[17] are used; however, there is some evidence that these predictions are too high by a factor of 2 for L electrons (Datla *et al.*).[18] This produces a large uncertainty in the predicted charge-state distribution. A major aim of our measurements is to determine the ionization cross-section values which produce the best agreement with experiment and to check the accuracy of calculations based on coronal equilibrium.

Figure 8 shows several Fe $K\alpha$ spectra from PLT at different temperatures. Each of these spectra was measured over a 125-msec long period, during which the central temperature on PLT was approximately constant [see Fig. 4(b)]. As $T_e(0)$ increases from 800 to >1800 eV, the centroid of the Fe $K\alpha$ intensity distribution increases from ~6550 to ~6660 eV and the predominant charge state increases from Fe XXI to Fe XXIV-XXV. In order to study the dependence of the charge state upon

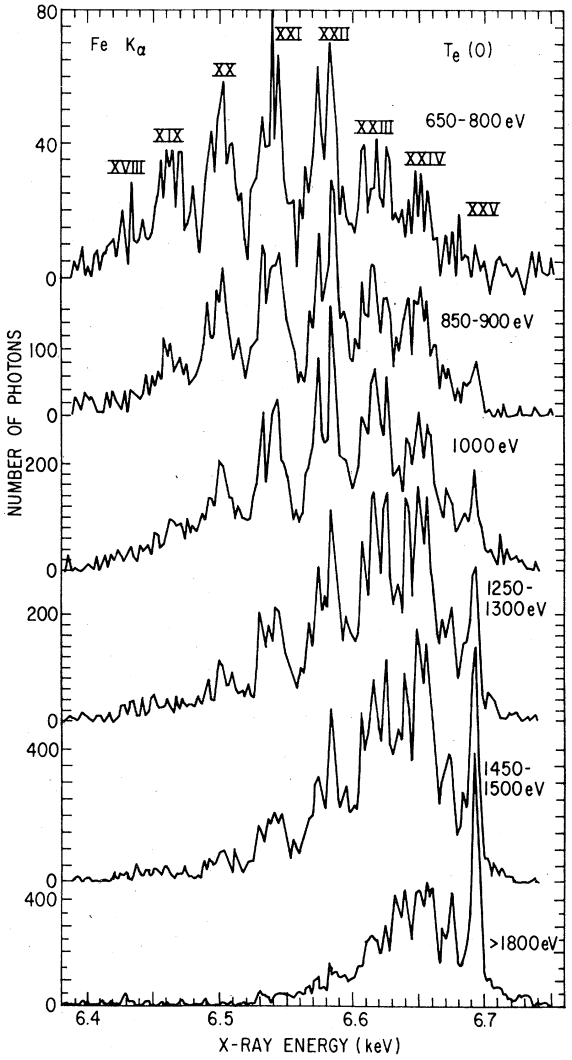

FIG. 8. Sample Fe $K\alpha$ or $1s$-$2p$ x-ray spectra taken from PLT plasma discharges. Each spectrum is a sum of from 8 to 25 spectra taken during different discharges. The spectra shown were accumulated only during the second time quadrant of the discharges, during which time the central electron temperature [$T_e(0)$], as determined by the pulse-height-analysis x-ray detector system, was approximately constant. The corresponding values of $T_e(0)$ for each spectrum are indicated. At $T_e(0) = 650$–850 eV, the charge states labeled Fe XX–Fe XXII (Fe^{19+}–Fe^{21+}) are the most abundant, while Fe XXIII–Fe XXV dominate the >1800-eV discharges.

$T_e(0)$, the fractional x-ray intensity under each major peak was compared with the calculated intensity.

This is shown in Fig. 9 for central electron temperatures $T_e(0)$ of 800, 1000, 1200, and 1500 eV. The shaded areas represent the experimental values; the dotted, the theoretical predictions. The intensities I_i were obtained by integrating mea-

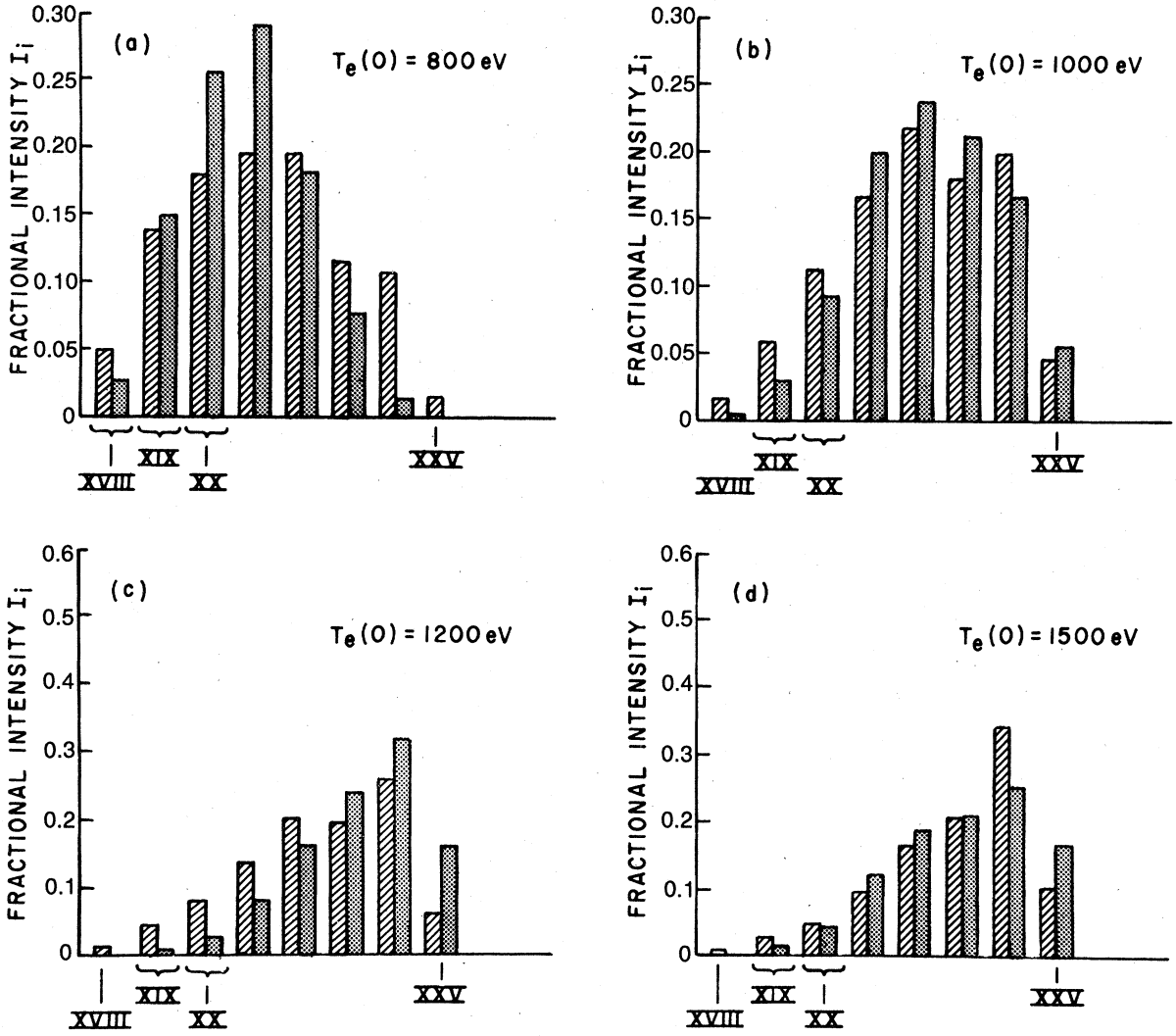

FIG. 9. Comparison of the measured fractional peak intensities in the eight major peak regions of Fe $K\alpha$ spectra from PLT (shaded curves) with the predictions of coronal-equilibrium calculations (dotted regions) for electron temperatures of (a) 800 eV, (b) 1000 eV, (c) 1200 eV, and (d) 1500 eV. For the calculations the L-shell ionization cross sections of Lotz (Ref. 17) were used for (a), (b), and (c), whereas $\frac{1}{2}$ the values of Lotz (as suggested in Ref. 18) were used in (d).

sured spectra over eight energy bands, which are marked by vertical lines in Fig. 6 and correspond mainly to the major charge-state peaks designated by Roman numerals, and by dividing by the total photon count. At the first three temperatures, the theoretical intensities were calculated with the L-shell ionization cross sections of Lotz,[17] whereas the values of Datla *et al.*[18] were used at 1500 eV. Thus, over the range $T_e = 800$–1500 eV, the Fe $K\alpha$ radiation from the central chord of the minor cross section of PLT is consistent with calculations based on the coronal equilibrium assumption, within the factor of 2 uncertainty in the L-shell ionization cross sections. However, we find in the data a systematic trend that the agreement is better with Lotz at low temperatures and better with Datla *et al.* at high temperatures, as if the ionization cross section per L-shell electron increases with the number of electrons in the L shell. This trend is expected since the binding energy per L-shell electron increases as more electrons are removed.

Differences between the theoretical and experimental intensity distributions of Fig. 9 can be attributed to several factors. These include plasma profile effects, overlapping spectral features

from more than one charge state, uncertainties in the theoretical ionization, excitation, and recombination rates, deviations of the plasma from coronal equilibrium, and contributions to the measured spectra from Cr $K\beta$ lines. Also, the 800-eV experimental distribution includes data from discharges with $T_e(0)$ ranging from 650 to 800 eV. This was done to improve statistics since the Fe $K\alpha$ intensity is low at these temperatures. This effect could contribute to the broadening of the 800-eV experimental distribution relative to the theoretical one.

Plasma profile effects result because the x rays are integrated along a line through the center of the minor cross section of the torus. While most of the radiation is produced in the hot central core of the discharge, part of it is emitted by ions in cooler regions just outside the core. This contribution should be small because the rates for excitation of the Fe $K\alpha$ radiation increase very strongly with temperature, and radial scans with the PHA system indicate that the radiation is emitted predominantly from the central core. Such profile effects tend to broaden the distribution of intensities and shift the envelope toward lower charge states. They probably are somewhat more important at higher temperatures.

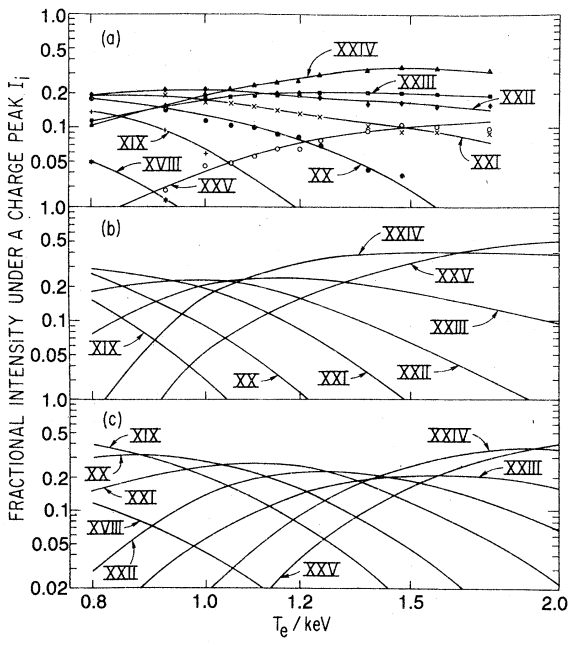

FIG. 10. (a). Measured fractional peak intensities vs electron temperature. Theoretical predictions by Merts, Cowan, and Magee (coronal equilibrium) are plotted in subfigures (b) and (c) using L-shell ionization cross sections of Lotz (Ref. 17) and $\frac{1}{2}$ Lotz (Ref. 18), respectively.

Deviation from coronal equilibrium results mainly from plasma transport. The equilibrium times for PLT discharges [$\bar{n}_e \approx (3\text{–}10)\times 10^{13}$ cm^{-3}] range typically from 0.5 to 3.0 msec. This pertains to charge states XVIII to XXIII. For charge states XXIV and XXV equilibrium times are considerably longer because dielectronic recombination is reduced. Comparing these values with typical numbers for the energy confinement time in PLT (20–70 msec), it is not surprising to find for the lower charge states close agreement with coronal equilibrium. The deviation of the experimental data at high temperatures from the calculation based on ionization cross sections of Lotz could be construed as a deviation from coronal equilibrium due to transport, although this effect is certainly within the accuracy with which we know these ionization cross sections.

The effects of Cr ($Z = 24$) $K\beta$ or $1s$-$3p$ radiation on the Fe ($Z = 26$) $K\alpha$ spectral intensities can only be estimated since detailed calculations are not available. Under the assumption that $K\beta$ x-ray energies for isoelectronic sequences similar to the two-electron sequence scale similarly with Z as for the $1s^2\,{}^1S$-$1s3p\,{}^3P^o$ transition,[19] the Fe $K\beta$ energies calculated (and in some cases measured) by Klapisch *et al.*[20] for Fe XXII – Fe XXV can be scaled to provide estimates of $K\beta$ energies for Cr XX – Cr XXIII. These energies fall in the 6400–6700 eV range of the Fe $K\alpha$ spectra. The Cr $K\beta$ lines, however, should have less than 5% of the intensity of the Fe $K\alpha$ lines since the Cr $K\alpha$ radiation measured by the PHA system [see Fig. 4(a)] is only about $\frac{1}{3}$ of the Fe $K\alpha$ intensity, and since the $K\beta/K\alpha$ intensity ratio for Cr and Fe is probably less than 0.1.

Another, perhaps more conventional, way of plotting the data is given in Fig. 10, where the fractional intensities of each of the eight charge-state peaks XVIII–XXV is graphed as a function of electron temperature T_e. Figures 10(b) and 10(c) are the theoretical predictions for intensities based on coronal equilibrium calculations using, respectively, the Lotz and $\frac{1}{2}$-Lotz L-shell ionization cross sections.

V. CONCLUSIONS

A Bragg curved-crystal spectrometer has been constructed to perform high-resolution spectroscopy of x-ray impurity lines. Using a multiwire proportional counter as the photon detector, we are able to obtain time- and energy-resolved measurements simultaneously. Thus, the problem of following one line component during one discharge and another component during a different discharge is not encountered. The resolving pow-

er of the instrument was approximately 1500 (i.e., 4 eV at a photon energy of 6400 eV).

With this instrument, the iron $1s$-$2p$ transition (Fe $K\alpha$) has been investigated. This is probably the most prominent impurity line in the soft x-ray spectra (1–20 keV) from PLT. The measured spectra are in excellent agreement with the detailed theoretical computer predictions of Cowan *et al.*[2,3] and conform well with spectra measured from solar flares[5] and laser-produced plasmas.[6]

The shape of the spectrum depends predominantly on the charge-state distribution of the iron ions which, in turn, depends practically only on electron temperature, according to coronal equilibrium models. Results from several hundred PLT discharges with central temperatures in the range 800–1500 eV indicate that coronal equilibrium is satisfied in the central region, within the factor of 2 uncertainty associated with the ionization cross sections used in the equilibrium computations.

ACKNOWLEDGMENTS

We thank Dr. H. P. Furth and Dr. M. Gottlieb for their continuing support. The authors gratefully acknowledge helpful discussions with Dr. A. J. Burek, Dr. R. Deslattes, Dr. A. Faessler, Dr. A. Henins, and Dr. E. Hinnov. One of us (K.W.H.) is especially grateful to Dr. W. Stodiek, Dr. L. A. Berry, and Dr. J. F. Clarke for making possible his visit to Princeton Plasma Plysics Laboratory while employed at Oak Ridge National Laboratory. We thank Dr. A. Favale and Dr. F. Kuehne for providing the multiwire proportional counter. The technical support of W. Mycock and M. Perron and his crew and the engineering help of J. Boychuk are gratefully acknowledged. This work has been supported by U.S. DOE-ERDA Contract No. EY-76-C-02-3073.

---

*Present address: Los Alamos Scientific Laboratory, Los Alamos, N.M.

†Present address: Racah Institute of Physics, The Hebrew University, Jerusalem, Israel.

[1]N. Bretz, D. Dimock, A. Greenberger, E. Hinnov, E. Meservey, W. Stodiek, and S. von Goeler, Princeton University Report MATT-1077 (1975) (unpublished); Plasma Phys. Contr. Nucl. Fus. Res. 1, 55 (1974).

[2]A. L. Merts, R. D. Cowan, and N. H. Magee, Jr., LASL Report LA-6220-MS (1976) (unpublished). More detailed computer outputs were provided by R. D. Cowan.

[3]R. D. Cowan (private communication).

[4]C. P. Bhalla, A. H. Gabriel, and L. P. Presnyakov, Mon. Not. R. Astron. Soc. 172, 359 (1975).

[5]Yu. I. Grineva, V. I. Karev, V. V. Korneev, V. V. Krutov, S. L. Mandelstam, L. A. Vainstein, B. N. Vasilyev, and I. A. Zhitnik, Solar Phys. 29, 441 (1973).

[6]Yu. A. Mikhailov, S. A. Pikuz. G. V. Sklizkov, A. Ya. Faenov, and S. I. Fedotov, Opt. Spectrosc. (USSR) 42, 469 (1977).

[7]H. Johann, Z. Phys. 69, 185 (1931).

[8]T. Johansson, Z. Phys. 82, 507 (1933).

[9]K. Feser and A. Faessler, Z. Phys. 209, 1 (1968).

[10]A. Favale, J. Dooher, W. Fischbein, F. Kuehne, M. Stauber, P. Suh, and F. Swanson, Grumman Research Department Report RE-423 (1972) (unpublished).

[11]Double-crystal-spectrometer rocking-curve measurements were made by A. J. Burek and A. Henins, National Bureau of Standards, Gaithersburg, Md.

[12]L. S. Birks, *Electron Probe Micronalysis*, 2nd ed. (Wiley-Interscience, New York, 1971), p. 47.

[13]G. F. Elwert, Naturforsch A 7, 432 (1952).

[14]A. Burgess, Astrophys. J. 139, 776 (1964); 141, 1588 (1965).

[15]C. Jordan, Mon. Not. R. Astron. Soc. 142, 501 (1969); 148, 17 (1970).

[16]A. H. Gabriel, Mon. Not. R. Astron. Soc. 160, 99 (1972).

[17]W. Lotz, Z. Phys. 206, 205 (1976); 216, 241 (1968).

[18]R. U. Datla, L. J. Nugent, and Hans R. Griem, Phys. Rev. A 14, 979 (1976).

[19]R. L. Kelly and L. J. Palumbo, NRL Report 7599 (1973). Available from the Superintendent of Documents, U. S. GPO, Washington, D.C. 20402, Stock No. 0851-00061.

[20]M. Klapisch, J. L. Schwob, B. S. Fraenkel, and J. Oreg, J. Opt. Soc. Am. 67, 148 (1977).

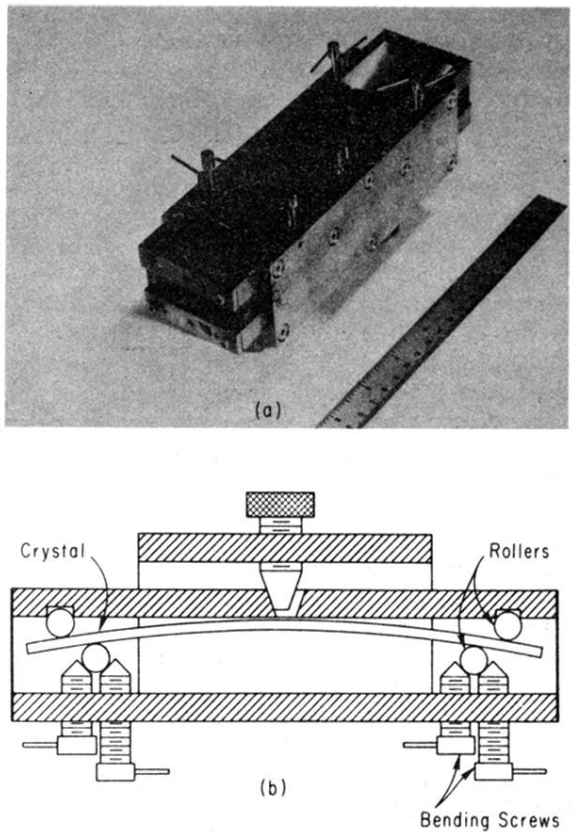

FIG. 2. (a) Photograph of the Ge(220) crystal in its bending jig. The crystal, two rollers, and eight screws for adjusting the radius of curvature can be seen. (b) Schematic cross-sectional illustration of crystal-bending jig showing a side view of the bent crystal slab. The two front (lower) cylindrical rollers press against the front (concave) surface of the crystal while the rear surface is held fixed by the two rear rollers. The radius of curvature of the crystal is adjusted by means of the fine-thread screws which hold the front rollers. The rear screw permits a lateral displacement of the rear rollers relative to the front ones so that the crystal can be bent to either a cylindrical or a logarithmic-spiral contour.